

PCCP

Accepted Manuscript



This is an *Accepted Manuscript*, which has been through the Royal Society of Chemistry peer review process and has been accepted for publication.

Accepted Manuscripts are published online shortly after acceptance, before technical editing, formatting and proof reading. Using this free service, authors can make their results available to the community, in citable form, before we publish the edited article. We will replace this *Accepted Manuscript* with the edited and formatted *Advance Article* as soon as it is available.

You can find more information about *Accepted Manuscripts* in the [Information for Authors](#).

Please note that technical editing may introduce minor changes to the text and/or graphics, which may alter content. The journal's standard [Terms & Conditions](#) and the [Ethical guidelines](#) still apply. In no event shall the Royal Society of Chemistry be held responsible for any errors or omissions in this *Accepted Manuscript* or any consequences arising from the use of any information it contains.

Tuning magnetism by biaxial strain in native ZnO

Chengxiao Peng,[†] Yuanxu Wang,^{*,†} Zhenxiang Cheng,^{*,†,‡} Guangbiao Zhang,[†]
Chao Wang,[†] and Gui Yang[†]

Institute for Computational Materials Science, School of Physics and Electronics, Henan University, Kaifeng, 475004, China, and Institute for Superconducting and Electronic Materials, University of Wollongong, Innovation Campus, Squires Way, Fairy Meadow, NSW 2519, Australia

E-mail: wangyx@henu.edu.cn; zxcheng@gmail.com

Abstract

Magnetic ZnO, as one of the most important diluted magnetic semiconductors (DMS), has attracted great scientific interest because of its possible technological applications in opto-magnetic devices. Magnetism in this material is usually delicately tuned by the doping level, dislocations, and local structures. The rational control of magnetism in ZnO is a highly attractive approach for practical applications. Here, the tuning effect of biaxial strain on the d^0 magnetism of native imperfect ZnO is demonstrated through first-principles calculations. Our calculation results show that strain conditions have little effect on the defect formation energy of Zn and O vacancies in ZnO, but they do affect the magnetism significantly. For a cation vacancy, increasing the compressive strain will obviously decrease its magnetic moment, while tensile strain can not change the moment, which remains constant at $2\mu_B$. For a singly charged anion vacancy, however, the dependence of the magnetic moment on strain is opposite to that

*To whom correspondence should be addressed

[†]Institute for Computational Materials Science, School of Physics and Electronics, Henan University, Kaifeng, 475004, China

[‡]Institute for Superconducting and Electronic Materials, University of Wollongong, Innovation Campus, Squires Way, Fairy Meadow, NSW 2519, Australia

of the Zn vacancy. Furthermore, the ferromagnetic state is always present, irrespective of strain type, for ZnO with two zinc vacancies, $2V_{\text{Zn}}$ s. A large tensile strain is favorable for improving the Curie temperature and realizing room temperature ferromagnetism for ZnO-based native semiconductors. For ZnO with two singly charged oxygen vacancies, $2V_{\text{O}}^+$ s, no ferromagnetic ordering can be observed. Our work points the way to rational design of materials beyond ZnO with novel non-intrinsic functionality by simply tuning the strain in a thin film form.

Introduction

In recent years, advances in the thin film technology, especially the ability to control layer-by-layer growth and the individual atomic positions have made thin film technology a powerful tool in the design of novel functional materials with properties that are not native to their bulk forms.¹ Such novel functionalities are mainly created at the hetero-interfaces of different materials due to spin, orbit, and charge reconstruction at the interface as a result of epitaxial growth and the substrate-clamping effect. Therefore strain in the interface of a film as a result of the substrate-clamping effect and film-substrate lattice mismatch is the decisive driving force for the appearance of induced functionality at the interface. It has been found that strain effects can lead to a substantial increase in mobility in transistors and in the superconducting, ferromagnetic (FM), and ferroelectric transition temperatures of many materials.² Strain can also affect the saturation magnetization and Curie temperature,³ and it even drives transitions from the antiferromagnetic to the ferromagnetic phase. Ma et al.'s results show that both the magnetic moment and the strength of magnetic coupling increase rapidly with increasing isotropic strain from -5% to 5% for VX_2 monolayers ($X = \text{S}, \text{Se}$).⁴ It was predicted for graphene monolayer that tensile strain along the zigzag direction could significantly enhance magnetic moments and the stability of FM coupling of graphene with a topological line defect.⁵ For half-fluorinated BN and GaN layers, applying strain could tune antiferromagnetism (AFM) to ferromagnetism.⁶ These studies show that strain has appeared as a powerful tool to tune magnetism in functional materials, both experimentally and theoretically.

ZnO-based dilute magnetic semiconductors have been extensively studied due to the pred-

ication of ferromagnetism above room temperature.^{7–11} Subsequently, ZnO d^0 ferromagnetism has been found to exist in undoped ZnO^{12–17} or in ZnO doped with non-magnetic ions, such as H,^{18–20} Li,^{21,22} C,^{23–25} and N.^{26,27} Based on both theoretical and experimental considerations, many groups have proposed that the ferromagnetism in nominally undoped ZnO arises from intrinsic defects. These defects include oxygen vacancy,^{13,15,28,29} zinc interstitial,^{13,15,28,30} zinc vacancy,^{12,14,21,31,32} and the defect complex of zinc vacancy and H interstitial,²⁰ as well as oxygen interstitial.³²

Experimentally, it has been shown that the substrates and annealing treatment have a substantial effect on d^0 magnetism in ZnO thin films. ZnO thin films with zinc vacancy grown on a , c , and r -plane sapphire, Si, quartz, and glass substrates show various saturated magnetization moments and types of magnetic behavior.¹⁴ Ong et al. reported that the saturation magnetization of the ZnO films decreased from about 4 to 0.6 emu/cm³ when they were grown on substrates in the following order: X-cut quartz, Y-cut quartz, and glass. No magnetic ordering was observed when ZnO films were grown on Z-cut quartz and silicon (001).³³ ZnO granular films deposited silicon substrates, however, after annealing in air at 500 and 800 °C, show significantly different saturated magnetizations, which is attributed to the relaxation of the intrinsic residual stress during the annealing process.³⁴ They found that Zn vacancies located at the interface have lower defect formation energy. Similarly, Zhan et al. showed that the reactions between epitaxial ZnO films and their silicon substrates give rise to the enhancement of ZnO ferromagnetism after annealing at 600 °C.²⁹ They proposed that the singly charged oxygen vacancy is the origin of ZnO d^0 ferromagnetism due to silicon atoms acting as traps for oxygen from ZnO films.

It is obvious that ZnO films doped with non-magnetic ions that were grown on different substrates and subjected to different heat-treatment conditions show a wide variety in their magnetism and saturation magnetizations. There is no doubt that the strain induced by the lattice mismatch between the substrate and the epitaxial film is the key factor in determining the magnetism of a material, so that a systematic quantitative study to show the role of strain in determining the d^0 magnetism in ZnO is highly desirable. In this work, we explore the effects of biaxial strain on

the origins of magnetism and magnetic intensity in native ZnO. Our investigations indicate that strain could effectively manipulate and control the magnetic moments of singly charged O vacancies and Zn vacancies. In addition, magnetic orders and coupling interactions could be tuned by various types of strain in native ZnO with defects. Thus, we prove that strain plays a crucial role in magnetic ordering and saturated magnetization for ZnO grown on different substrates (or crystal planes), and the variation in the magnetic ordering and saturated magnetization after annealing has a close relationship with strain relief. Furthermore, our results demonstrate that strain can then be used as a powerful tool in quantitative adjustment of the d^0 magnetism of ZnO material and beyond, making it possible to realize rational design of materials for desired functionalities.

Methods

The present first-principles calculations are based on spin-polarized density functional theory (DFT) using the generalized gradient approximation (GGA) for the exchange-correlation potential given by the Perdew-Burke-Ernzerhof (PBE) exchange-correlation functional.³⁵ All calculations were performed by using the Vienna *ab initio* simulation package (VASP),^{36,37} with the projector augmented-wave (PAW) potential.³⁸ The ZnO epitaxial film is modeled with a $3 \times 3 \times 2$ periodic supercell which contains 72 atoms. The zinc (oxygen) vacancy was constructed by removing one zinc (oxygen) atom from the supercell, with the resultant vacancy labeled as $V_{\text{Zn}}(V_{\text{O}})$. The plane-wave energy cut-off was set at 450 eV, and a $3 \times 3 \times 3$ k-point mesh was adopted for integration in the first Brillouin zone. In all the calculations, self-consistency was achieved with a tolerance in the total energy of at least 1.0×10^{-6} eV. The Hellman-Feynman force components on each ion were made to converge to less than 0.01 eV/Å. In our calculations, considering the substrate-clamping effect in real film growth, we fixed the lattice constants of the a and b axes ($a = b$) for each strain, while relaxing the c -axis length and all internal coordinates. From the relaxation of c values and the total energy E , the optimal c value was fitted. We defined the biaxial strain as $\varepsilon = (a_0 - a)/a_0 \times 100\%$, where a_0 and a are the lattice constants of the perfect ZnO bulk in

its equilibrium and strained states, respectively. For the investigation of magnetic coupling, we constructed a $6 \times 3 \times 2$ periodic supercell containing $2V_{Zn}$ s ($2V_{O}^+$ s).

The standard approximations to the exchange-correlation energy, *i.e.*, the local-density approximation LDA as well as GGA, often fail to describe systems with strongly localized *d* or *f* electrons.³⁹ Therefore, the hybrid functionals, such as PBE0 and HSE06, obtained by admixing a fixed amount of the Fock exchange, presents a significant improvement over the GGA(LDA) description materials properties. Unfortunately, hybrid functionals method often spend largely computational resources and more time.

Besides hybrid functionals to correct the drawbacks of LDA(GGA) method, +U is often another choice. Since the *3d* electrons on the transition metal atoms are presumably strongly correlated, the onsite Coulomb energy U was taken into account with the so-called LDA(GGA)+U scheme. The experimental report on the location of Zn *3d* states varies from 7.5 to 8.8 eV below the valence band maxima.⁴⁰ Hence, we set the effective U value 7.5 eV for Zn *3d* electrons. The corresponding parameters U and J used for our calculations is $U-J = 7.5$ eV.

We use the PBE0 hybrid-functional and GGA+U to evaluate the magnetic results obtained with a GGA method. The magnetic moment of Zn vacancy varies from $2\mu_B$ to 1.59 (1.45) μ_B corresponding to 0 and 5% strain with a PBE0 and GGA+U method, respectively. The magnetic moment decreases with the increase of compressive strain. However, the variation range obviously decreases. DFT approaches underestimate the binding energy of the semicore *d* states and consequently overestimate their hybridization with the anion *p*-derived valence states, enhancing the effects of the *p-d* coupling. When an on-site Coulomb correction has been applied on the Zn *3d* orbitals, the hybridization of Zn *3d* with the O *2p* electrons weakens. The Zn *d*-orbitals which hybridized with those of O *p*-orbitals resulting in delocalization in GGA has been recovered to more localized state. O *2p* electrons around Zn vacancy vary weakly without the hybridization of Zn *3d* electrons under different strain. The decrease trend of magnetic moment for Zn vacancy keeps with increasing compressive strain. Therefore, strain still has a tuning effect on magnetic moment irrespective of PBE0 or GGA+U method. All results and discussion in the following sections are

obtained with GGA method.

Results and Discussion

Effects of strain on the defect formation energy and magnetic moments of defects in ZnO

The formation energy of a point defect in ZnO depends on the relative abundance of Zn and O atoms, i.e., the chemical potentials μ_{Zn} and μ_{O} . The formation energy of defect α with a charge q is:⁴¹ $E^f(q, \alpha) = E_{\text{tot}}(q, \alpha) - E_{\text{tot}}(\text{ZnO}) + n_{\alpha}\mu_{\alpha} + q(E_{\text{F}} + E_{\text{V}} + \Delta V)$, where $E_{\text{tot}}(q, \alpha)$ is the total energy of the supercell containing the defect α in charge state q , $E_{\text{tot}}(\text{ZnO})$ is the total energy of a ZnO perfect crystal in the same supercell, μ_{α} is the chemical potential of the α element. n_{α} is the number of atoms removed during the defect formation from the host crystal, with a sign that can be positive and vice versa. E_{F} is the Fermi energy, and E_{V} is the valence-band maximum of the host crystal. ΔV aligns the reference potential in a one-defect supercell with that in the bulk. For a neutral Zn vacancy defect, its formation energy could be written as: $E^f(\text{V}_{\text{Zn}}) = E_{\text{tot}}(\text{V}_{\text{Zn}}) - E_{\text{tot}}(\text{ZnO}) + \mu_{\text{Zn}}$. A similar expression could be written for a neutral O vacancy. For a singly charged oxygen vacancy, its formation energy expression is as follows: $E^f(\text{V}_{\text{O}}^+) = E_{\text{tot}}(\text{V}_{\text{O}}^+) - E_{\text{tot}}(\text{ZnO}) + \mu_{\text{O}} + E_{\text{F}} + E_{\text{V}} + \Delta V$. Limited by the thermodynamic stability condition for ZnO, Zn and O are variables correlated as $\mu_{\text{Zn}} + \mu_{\text{O}} = \Delta H(\text{ZnO})$, where $\Delta H(\text{ZnO})$ is the enthalpy of formation of bulk ZnO. The calculated formation enthalpy of ZnO is -2.90 eV, which is close to -2.93 eV⁴² and is smaller than the experimental value of -3.61 eV.⁴³ Under the O rich limit condition, $\mu_{\text{O}} = 1/2E_{\text{O}_2}$, $\mu_{\text{Zn}} = \Delta H(\text{ZnO}) - 1/2E_{\text{O}_2}$; similarly, under the Zn rich limit condition, $\mu_{\text{Zn}} = E_{\text{Zn}}$, $\mu_{\text{O}} = \Delta H(\text{ZnO}) - E_{\text{Zn}}$.

Figure 1 shows the defect formation energy and magnetic moments of a Zn vacancy and a singly charged oxygen vacancy V_{O}^+ under different strain conditions. For neutral V_{Zn} and V_{O} under no biaxial strain condition, their formation energy is 5.3(2.4) eV and 0.81(3.71) eV under rich Zn(O) conditions, respectively. Our calculations are in good agreement with the reported

data.^{20,27,44} For neutral V_{Zn} and V_O , the variation in their formation energy is in the range of 0.3 eV under compressive and tensile strain conditions, in contrast to that under no biaxial strain. For a singly charged oxygen vacancy V_O^+ , the formation energy is a function of the shift of the Fermi energy level. Here, we suppose that ZnO is in a *p*-type condition and the shift of the Fermi energy level is set to zero. The variation in the range of its formation energy is 0.6 eV with respect to the original structure. According to $n = N_{sites} \exp(E^f/k_B T)$, where E^f is the defect formation energy, we can roughly estimate the variations in defect concentration, n , with strain for different defects. Compared with no strain, the defect concentration increases by no more than 1 order of magnitude for V_{Zn} and V_O at the temperature of 1500 K under strain conditions. The V_O^+ defect concentration only increases by 2 orders of magnitude at 1500 K due to its lower defect formation energy. Therefore, biaxial strain in ZnO epitaxial thin films has little influence on the defect formation, and this is quite different from the case of ZnO subjected to hydrostatic stress, in which the defect concentration could increase by 9 orders of magnitude.⁴⁴

The magnetic moments are in good agreement with the 0, 1, and 2 μ_B , corresponding to 0, 1, and 2 unpaired electrons for a neutral V_O , V_O^+ , and V_{Zn} , respectively. The magnetic moment for V_{Zn} remains almost at 2 μ_B in the range of tensile strain, and it dramatically decreases under the compressive strain condition, in contrast to V_O^+ .

ZnO containing a Zn vacancy (V_{Zn}) without and with strain

Fig. 2 shows the (000 $\bar{1}$) face spin charge density for ZnO containing a V_{Zn} with no biaxial strain, which is magnified 2 times along the *a* and *b* axes on the base of the original supercell structure. The spin charges mainly surround the four nearest-neighbor oxygen atoms around the zinc vacancy, and they are larger for the three O atoms in the *ab*-plane than for the O along the *c* direction. The corresponding magnetic moments are 0.184 and 0.129 μ_B . The shapes of the spin charges for the three O atoms in the *ab*-plane resemble dumbbells and are the same, while the spin charge distribution is perpendicular to the *ab*-plane for the O along the *c* axis. The shapes of the spin charges indicate that the 2p_x and 2p_y orbitals have hybridized and have made the greatest contribution to

the magnetic moments for the three oxygen atoms in the ab -plane. For the oxygen atom along the c -axis, however, the $2p_z$ orbitals provides the greatest contribution to its magnetic moment. The three second nearest-neighbor oxygen atoms in the ab -plane have magnetic moments of $0.011 \mu_B$, while the three third nearest-neighbor oxygen atoms in the ab -plane have magnetic moments of $0.064 \mu_B$. The difference between the magnetic moments for second nearest-neighbors and third nearest-neighbors is in agreement with the spin charge distribution. One of the third nearest-neighbors is between two nearest-neighbors in Fig. 2, and these oxygen atoms are magnetized. It is noteworthy that the shapes of the spin charges for the magnetized oxygen atoms depend on their adjacent atoms. The magnetization is transmitted and the magnetization intensity is sharply damped.

Fig. 3 (a-e) shows the $(000\bar{1})$ face spin charge density for ZnO containing a V_{Zn} with various strain, i.e., $\epsilon = -5\%$ (a), $\epsilon = 0\%$ (b), $\epsilon = 1\%$ (c), $\epsilon = 3\%$ (d), and $\epsilon = 5\%$ (e). In Fig. 1(a), the magnetic moment for the supercell with a tensile strain has increased a little in contrast to the supercell with no external strain. Compared with Fig. 3(b), the spin charge density around the Zn atoms is clearly strengthened in Fig. 3(a). With increasing compressive strain, the isosurfaces around the nearest-neighbor O atoms and 3^{rd} -nearest-neighbor O atoms become vestigial, and especially in the case of the O10 atom, its isosurface is quickly reduced and finally disappears. The number of spin-up electrons on 2^{nd} -nearest-neighbor O atoms gradually decreases, and their orientation reverse, which weakens the magnetic moment for the supercell. In addition, the spin charge distribution around the Zn atoms gradually disappears.

The magnetic moments mainly come from the nearest-neighbor oxygen atoms around the Zn vacancy for ZnO with a V_{Zn} . According to Fig. 2(a), the electrons surrounding O atoms are spin-up, and these unpaired electrons of oxygen atoms determine their magnetic moments. The interactions among the nearest-neighbor oxygen atoms play a crucial role in tuning the unpaired electrons. When this system is under compressive strain conditions, the hybridizations of the nearest-neighbor oxygen atoms are strengthened, and therefore, a part of the spin-up electrons reverse their orientation and become spin-down in order to lower the system energy. It is clearly

observed that the electron spins are turning down in the spin charge density distributions from Fig. 3(b) to (e). The number of spin-up electrons of the 2nd-nearest-neighbor oxygen atoms around V_{Zn} decreases, and the electrons obviously reverse their spin, which results in the reduced magnetic moment for the compressive ZnO system. Under tensile conditions, the reduction of electron overlapping of the nearest-neighbor oxygen atoms leads to constant unpaired electrons in contrast to zero strain, so that the magnetic moments almost remain unchanged under tensile conditions.

The spin-slip of spin-up electrons can be further confirmed in Fig. 4, which shows the density of states(DOS) for ZnO containing a V_{Zn} with $\epsilon = 5\%$, $\epsilon = 0\%$, and $\epsilon = -5\%$ strain. The Fermi energy level only crosses the spin-down valence band under the $\epsilon = -5\%$ strain condition, while it crosses both the spin-up and spin-down valence bands under the $\epsilon = 5\%$ strain condition. Total electrons, including spin-up and spin-down electrons, in the supercell under various strain are the same and occupy the levels below the Fermi level. The levels are empty above the Fermi level. The spin-up and spin-down channels could accumulate the same number of electrons below $E_F+0.5$ eV. Thus, the total unfilled states, including spin-up and spin-down, should be equal for the cases of different strain cases in the region of between E_F and $E_F+0.5$ eV. Compared to Fig. 4(b), the spin-down empty states decrease, and the spin-up empty states increase in Fig. 4(a). This means that the number of spin-down electrons increases and the number of spin-up electrons decreases. Thus, the spin-flip of the spin-up electrons occurs under compressive strain. The DOS of the spin-up and spin-down electrons almost remains unchanged under tensile strain in contrast to zero strain, which is in agreement with the variation in magnetic moments.

ZnO containing a V_O^+ without and with strain

Fig. 5 shows the spin charge density of ZnO with a V_O^+ under $\epsilon = 0\%$ and $\epsilon = -1\%$ strain. The electrons are mainly localized at the V_O^+ site, while they are distributed at the nearest oxygen atoms around the Zn vacancy in the ZnO systems with a V_{Zn} . The difference in the charge distribution is primarily due to the large electronegativity for O in contrast to Zn. The number of spin-up electrons in the ZnO system with one V_O^+ under $\epsilon = -1\%$ strain decreases significantly in contrast to

$\varepsilon = 0\%$. Moreover, more spin-down electrons are localized around the nearest-neighbor Zn atoms. This means that there has a remarkable increase the number of spin-down electrons. The electrons around V_O^+ come from the surrounding Zn atoms, and the electrons are localized due to the repulsion by surrounding O atoms. The repulsion by the surrounding O atoms is significantly weakened under tensile strain, thus, the spin-up localized electrons escape into the surrounding crystal space. These localized electrons at V_O^+ substantially delocalize, which induces a few spin-down electrons to be present due to the Pauli Exclusion Principle. There is a charge transfer from the spin-up to spin-down channels. Under compressive strain, localized electrons at V_O^+ are still localized due to the larger repulsion by surrounding O atoms. The unpaired spin-up electrons almost remain constant under compressive strain, and therefore, the corresponding magnetic moments for ZnO with a V_O^+ hardly change.

To further illustrate the effects of tensile strain on the magnetic properties of ZnO with a V_O^+ , the density of states for ZnO containing a V_O^+ for $\varepsilon = 0\%$ and $\varepsilon = -1\%$ strain is shown in Fig. 6(a) and (b), respectively. The DOS for spin-up and spin-down electrons near the Fermi level changes from up-down asymmetric to up-down symmetric as the tensile strain increases. In addition, the spin-up electrons near the Fermi level absolutely prevail in ZnO containing a V_O^+ without strain, while they significantly decrease and change their spin orientation when 1% tensile strain is applied to the ZnO system. This is consistent with the change in the spin charge distribution in Fig. 5.

Magnetic coupling tuned by strain in ZnO containing two V_{Zn} s (V_O^+ s)

Considering the practical applications, materials with a long-range ferromagnetic ordering are highly desirable. Hence, we investigated the more stable states among the ferromagnetic (FM) state, antiferromagnetic (AFM) state, and paramagnetic (PM) state. The corresponding energy difference $\Delta E (\Delta E = E_{FM} - E_{AFM})$ for ZnO with two V_{Zn} s as a function of strain is illustrated in Table 1. We considered a short-range 6.58 Å and a long-range 9.83 Å defect distance between two Zn vacancies, respectively. For two cases, the energy difference, ΔE , effectively decreases with higher compression, and the ferromagnetic state is always more stable than the AFM state for ZnO

with two V_{Zn} s. Correspondingly, the ferromagnetic coupling could be quenched with compressive stress. According to the mean-field theory and the Heisenberg model, we can roughly estimate the Curie temperature T_C using $k_B T_C = (2/3)\Delta E$.⁴⁵⁻⁴⁷ When the defect distance is a long-range 9.83 Å, the calculated T_C under 5% and -5% strain is 116 K and 294 K, respectively. Strong magnetic coupling interaction under tensile strain results in a high Curie temperature. It is obvious that large tensile strain is favorable for improving the Curie temperature and realizing room temperature ferromagnetism for ZnO-based native semiconductors.

It is clear that the coupling interaction between two Zn vacancies strongly depends on the defect distance. With the distance between two Zn vacancies elongated under a fixed strain, the ferromagnetic coupling between two Zn vacancies decreases. As is shown in the spin charge density in Fig.2, the spin charges are delocalized around the Zn vacancy. When the distance between two Zn vacancies is elongated, the overlap of spin charge reduces, the ferromagnetic coupling interaction weakens. On the other hand, when the compression is applied on ZnO with a Zn vacancy, the distance between two Zn vacancies is shortened. But the shortening of defect distance under 5% compressive strain is so little, the preponderant effect on ferromagnetic coupling is the deformation under the compressive strain. With the increasing of compressive strain at a fixed defect distance, the magnetic moment of oxygen atoms around Zn vacancy is reduced. Therefore, the weakened ferromagnetic coupling is observed.

The exchange mechanism could be understood through the spin charge distribution in Fig. 2. The spin charge distribution is delocalized around the Zn vacancy, and the ferromagnetic coupling is present through the delocalized electrons. This long distance ferromagnetic coupling maybe occur on the base of local moments around Zn vacancy through conduction electrons prolonging like RKKY theory.

For ZnO with $2V_{\text{O}}^+$ s, we compare the energies for the FM, AFM, and PM states. The calculated findings show that the AFM state is more stable than the FM state without strain and under compressive strain. The FM state behaves as a metastable state, and its energy is 21 meV higher than that of the AFM state without strain. With increasing compressive strain, ΔE is reduced. While

tensile strain is applied, the ground state for ZnO with $2V_{\text{O}}^+$ s prefers to be a PM state. As mentioned above, the ferromagnetic state is not a stable state, regardless of the presence or absence of strain, for ZnO with $2V_{\text{O}}^+$ s. Therefore, the V_{O}^+ defect is not a possible origin of the native ZnO d^0 ferromagnetism.

Ma et al.⁴ successfully proposed that the variation in the energy difference between the AFM and FM states with strain arises from the competition between through-bond interaction and through-space interaction. The through-bond interaction leads to a ferromagnetic coupling, but the through-space interaction results in an antiferromagnetic coupling. The increase in the through-space interaction is larger than the increase in the through-bond interaction for ZnO with two V_{Zn} s under compressive strain. The competition between the two interactions could effectively explain the reduction in the energy difference between AFM and FM with increasing compressive strain.

For ZnO with two V_{O}^+ s, the ground state is the AFM state without and with compressive strain due to the possibly predominant through-space coupling interaction. When the material is under tensile strain, the exchange interactions among atoms decrease and even vanish with the increasing distance between atoms. Thus, the ground state is a PM state under tensile strain.

Conclusion

Tensile and compressive strain could effectively modulate magnetic properties of ZnO with native defects. The response of the magnetic properties of ZnO with a V_{Zn} or a V_{O}^+ to strain could be attributed to the electron interactions among the remaining atoms around a vacancy. Further studies show that the ground state for ZnO with two V_{Zn} s is always a ferromagnetic state. Under -5% tensile strain the estimated Curie temperature is 294 K, reaching room temperature. Hence, the Zn vacancy plays an important role in native ZnO room temperature d^0 ferromagnetism. The competition between through-bond and through-space interactions could effectively explain the reduction in the energy difference between AFM and FM as the compressive strain increasing. On the other hand, for ZnO with two V_{O}^+ s, no ferromagnetic state is observed. Hence V_{O}^+ is excluded as an origin of ferromagnetism in ZnO. The considerably different ferromagnetic intensities for

ZnO grown on various substrates may arise from the different strain that exist in the films. In addition, the strain tuning of the magnetism of ZnO with intrinsic defects has a great advantage for achieving homogeneity in the material and will pave the way to controllable spintronics.

Acknowledgement

This research was sponsored by the National Natural Science Foundation of China (No. 11305046, 21071045), foundation of Henan Educational Committee (No.13A140076), the Program for New Century Excellent Talents in University (No. NCET-10-0132), the Program for Innovative Research Team (in Science and Technology) in University of Henan Province (No. 13IRTSTHN017).

References

1. Ederer, C.; Spaldin, N. A. Influence of strain and oxygen vacancies on the magnetoelectric properties of multiferroic bismuth ferrite. *Physical Review B* **2005**, *71*, 224103.
2. Lee, J. H.; Fang, L.; Vlahos, E.; Ke, X.; Jung, Y. W.; Kourkoutis, L. F.; Kim, J.-W.; Ryan, P. J.; Heeg, T.; Roeckerath, M. et al. A strong ferroelectric ferromagnet created by means of spin-lattice coupling. *Nature* **2010**, *466*, 954–958.
3. Gan, Q.; Rao, R.; Eom, C.; Garrett, J.; Lee, M. Direct measurement of strain effects on magnetic and electrical properties of epitaxial SrRuO₃ thin films. *Applied Physics Letters* **1998**, *72*, 978–980.
4. Ma, Y.; Dai, Y.; Guo, M.; Niu, C.; Zhu, Y.; Huang, B. Evidence of the existence of magnetism in pristine VX₂ monolayers (X = S, Se) and their strain-induced tunable magnetic properties. *ACS Nano* **2012**, *6*, 1695–1701.
5. Kou, L.; Tang, C.; Guo, W.; Chen, C. Tunable magnetism in strained graphene with topological line defect. *ACS Nano* **2011**, *5*, 1012–1017.

6. Ma, Y.; Dai, Y.; Guo, M.; Niu, C.; Yu, L.; Huang, B. Strain-induced magnetic transitions in half-fluorinated single layers of BN, GaN and graphene. *Nanoscale* **2011**, *3*, 2301–2306.
7. Dietl, T.; Ohno, H.; Matsukura, F.; Cibert, J.; Ferrand, D. Zener model description of ferromagnetism in zinc-blende magnetic semiconductors. *Science* **2000**, *287*, 1019–1022.
8. Fukumura, T.; Jin, Z.; Kawasaki, M.; Shono, T.; Hasegawa, T.; Koshihara, S.; Koinuma, H. Magnetic properties of Mn-doped ZnO. *Applied Physics Letters* **2001**, *78*, 958–960.
9. Ueda, K.; Tabata, H.; Kawai, T. Magnetic and electric properties of transition-metal-doped ZnO films. *Applied Physics Letters* **2001**, *79*, 988–990.
10. Fukuma, Y.; Odawara, F.; Asada, H.; Koyanagi, T. Effects of annealing and chemical doping on magnetic properties in Co-doped ZnO films. *Physical Review B* **2008**, *78*, 104417.
11. Cheng, Z.; Wang, X.; Dou, S.; Ozawa, K.; Kimura, H.; Munroe, P. Fabrication, Raman spectra and ferromagnetic properties of the transition metal doped ZnO nanocrystals. *Journal of Physics D: Applied Physics* **2007**, *40*, 6518.
12. Sanyal, D.; Roy, T. K.; Chakrabarti, M.; Dechoudhury, S.; Bhowmick, D.; Chakrabarti, A. Defect studies in annealed ZnO by positron annihilation spectroscopy. *Journal of Physics: Condensed Matter* **2008**, *20*, 045217.
13. Zhang, X.; Cheng, Y.; Li, L.; Liu, H.; Zuo, X.; Wen, G.; Li, L.; Zheng, R.; Ringer, S. Evidence for high-T_c ferromagnetism in Zn_x(ZnO)_{1-x} granular films mediated by native point defects. *Physical Review B* **2009**, *80*, 174427.
14. Khalid, M.; Ziese, M.; Setzer, A.; Esquinazi, P.; Lorenz, M.; Hochmuth, H.; Grundmann, M.; Spemann, D.; Butz, T.; Brauer, G. et al. Defect-induced magnetic order in pure ZnO films. *Physical Review B* **2009**, *80*, 035331.
15. Zhang, Y.; Xie, E. Nature of room-temperature ferromagnetism from undoped ZnO nanoparticles. *Applied Physics A* **2010**, *99*, 955–960.

16. Podila, R.; Queen, W.; Nath, A.; Arantes, J. T.; Schoenhalz, A. L.; Fazzio, A.; Dalpian, G. M.; He, J.; Hwu, S. J.; Skove, M. J. et al. Origin of FM ordering in pristine micro-and nanostructured ZnO. *Nano Letters* **2010**, *10*, 1383–1386.
17. Hong, J.-I.; Choi, J.; Jang, S. S.; Gu, J.; Chang, Y.; Wortman, G.; Snyder, R. L.; Wang, Z. L. Magnetism in dopant-free ZnO nanoplates. *Nano Letters* **2012**, *12*, 576–581.
18. Sanchez, N.; Gallego, S.; Cerdá, J.; Muñoz, M. Tuning surface metallicity and ferromagnetism by hydrogen adsorption at the polar ZnO (0001) surface. *Physical Review B* **2010**, *81*, 115301.
19. Li, T.; Ong, C.; Heng, T.; Yi, J.; Bao, N.; Xue, J.; Feng, Y.; Ding, J. Surface ferromagnetism in hydrogenated-ZnO film. *Applied Physics Letters* **2011**, *98*, 152505–152505.
20. Peng, C.; Liang, Y.; Wang, K.; Zhang, Y.; Zhao, G.; Wang, Y. Possible origin of ferromagnetism in an undoped ZnO d0 semiconductor. *The Journal of Physical Chemistry C* **2012**, *116*, 9709–9715.
21. Yi, J.; Lim, C.; Xing, G.; Fan, H.; Van, L.; Huang, S.; Yang, K.; Huang, X.; Qin, X.; Wang, B. et al. Ferromagnetism in dilute magnetic semiconductors through defect engineering: Li-doped ZnO. *Physical Review Letters* **2010**, *104*, 137201.
22. Chen, Y.; Song, Q.; Yan, H. Ferromagnetic properties, electronic structures, and formation energies of Zn vacancy monodoping and (Zn vacancy, Li) codoped ZnO by first principles study. *Computational Materials Science* **2011**, *50*, 2157–2161.
23. Pan, H.; Yi, J.; Shen, L.; Wu, R.; Yang, J.; Lin, J.; Feng, Y.; Ding, J.; Van, L.; Yin, J. Room-temperature ferromagnetism in carbon-doped ZnO. *Physical Review Letters* **2007**, *99*, 127201.
24. Gao, F.; Hu, J.; Wang, J.; Yang, C.; Qin, H. Ferromagnetism induced by intrinsic defects and carbon substitution in single-walled ZnO nanotube. *Chemical Physics Letters* **2010**, *488*, 57–61.

25. Botello-Méndez, A. R.; López-Urías, F.; Terrones, M.; Terrones, H. Effect of impurities on the electronic and magnetic properties of zinc oxide nanostructures. *Chemical Physics Letters* **2010**, *492*, 82–88.
26. Xu, H.; Rosa, A.; Frauenheim, T.; Zhang, R. N-doped ZnO nanowires: Surface segregation, the effect of hydrogen passivation and applications in spintronics. *Physica Status Solidi B: Basic Solid State Physics* **2010**, *247*, 2195–2201.
27. Fang, D.; Rosa, A.; Zhang, R.; Frauenheim, T. Theoretical exploration of the structural, electronic, and magnetic properties of ZnO nanotubes with vacancies, antisites, and nitrogen substitutional defects. *The Journal of Physical Chemistry C* **2010**, *114*, 5760–5766.
28. Mishra, D.; Kumar, P.; Kumar Sharma, M.; Das, J.; Singh, S.; Roul, B.; Varma, S.; Chatterjee, R.; Srinivasu, V.; Kanjilal, D. Ferromagnetism in ZnO single crystal. *Physica B: Condensed Matter* **2010**, *405*, 2659–2663.
29. Zhan, P.; Wang, W.; Xie, Z.; Li, Z.; Zhang, Z.; Zhang, P.; Wang, B.; Cao, X. Substrate effect on the room-temperature ferromagnetism in un-doped ZnO films. *Applied Physics Letters* **2012**, *101*, 031913.
30. Heng, T.; Lau, S.; Yu, S.; Chen, J.; Teng, K. Zn-interstitial-enhanced ferromagnetism in Cu-doped ZnO films. *Journal of Magnetism and Magnetic Materials* **2007**, *315*, 107–110.
31. Xing, G.; Lu, Y.; Tian, Y.; Yi, J.; Lim, C.; Li, Y.; Li, G.; Wang, D.; Yao, B.; Ding, J. et al. Defect-induced magnetism in undoped wide band gap oxides: Zinc vacancies in ZnO as an example. *AIP Advances* **2011**, *1*, 022152.
32. Zuo, X.; Yoon, S.-D.; Yang, A.; Duan, W.-H.; Vittoria, C.; Harris, V. G. Ferromagnetism in pure wurtzite zinc oxide. *Journal of Applied Physics* **2009**, *105*, 07C508–07C508.
33. Ong, C.; Heng, T.; Huang, X.; Feng, Y.; Ding, J. Strain-induced ZnO spinterfaces. *The Journal of Physical Chemistry C* **2012**, *116*, 610–617.

34. Xu, X.; Xu, C.; Chen, G.; Wu, J.; Hu, J. Role of zinc vacancies in driving ferromagnetism in undoped ZnO granular films. *Europhysics Letters* **2013**, *101*, 27009.
35. Perdew, J. P.; Burke, K.; Ernzerhof, M. Generalized gradient approximation made simple. *Physical Review Letters* **1996**, *77*, 3865.
36. Kresse, G.; Furthmüller, J. Efficient iterative schemes for ab initio total-energy calculations using a plane-wave basis set. *Physical Review B* **1996**, *54*, 11169.
37. Kresse, G.; Joubert, D. From ultrasoft pseudopotentials to the projector augmented-wave method. *Physical Review B* **1999**, *59*, 1758.
38. Blöchl, P. E. Projector augmented-wave method. *Physical Review B* **1994**, *50*, 17953.
39. Wróbel, J.; Kurzydłowski, K. J.; Hummer, K.; Kresse, G.; Piechota, J. Calculations of ZnO properties using the Heyd-Scuseria-Ernzerhof screened hybrid density functional. *Physical Review B* **2009**, *80*, 155124.
40. Oba, F.; Togo, A.; Tanaka, I.; Paier, J.; Kresse, G. Defect energetics in ZnO: A hybrid Hartree-Fock density functional study. *Physical Review B* **2008**, *77*, 245202.
41. Van de Walle, C. G.; Neugebauer, J. First-principles calculations for defects and impurities: Applications to III-nitrides. *Journal of Applied Physics* **2004**, *95*, 3851–3879.
42. Lany, S.; Zunger, A. Dopability, intrinsic conductivity, and nonstoichiometry of transparent conducting oxides. *Physical Review Letters* **2007**, *98*, 045501.
43. Dean, J. A., Ed. *Langeq's Handbook of Chemistry. 14th Edition.*; McGraw-Hill:New York, 1992.
44. Kan, E.; Wu, F.; Zhang, Y.; Xiang, H.; Lu, R.; Xiao, C.; Deng, K.; Su, H. Enhancing magnetic vacancies in semiconductors by strain. *Applied Physics Letters* **2012**, *100*, 072401.

45. Kudrnovský, J.; Turek, I.; Drchal, V.; Mácá, F.; Weinberger, P.; Bruno, P. Exchange interactions in III-V and group-IV diluted magnetic semiconductors. *Physical Review B* **2004**, *69*, 115208.
46. Jin, H.; Dai, Y.; Huang, B.; Whangbo, M.-H. Ferromagnetism of undoped GaN mediated by through-bond spin polarization between nitrogen dangling bonds. *Applied Physics Letters* **2009**, *94*, 162505.
47. Shi, H.; Pan, H.; Zhang, Y.-W.; Yakobson, B. I. Strong ferromagnetism in hydrogenated monolayer MoS₂ tuned by strain. *Physical Review B* **2013**, *88*, 205305.

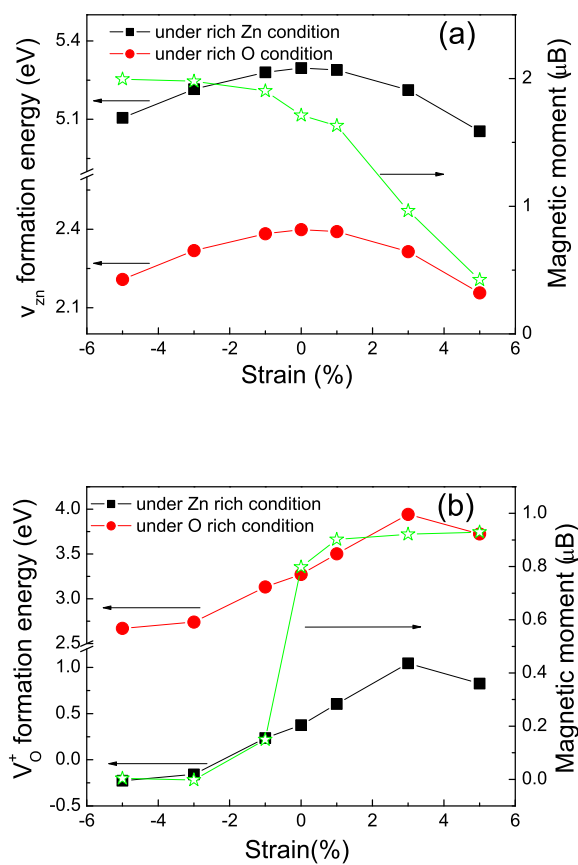


Figure 1: Variation of defect formation energy and magnetic moments with strain for V_{Zn} (a) and V_O^+ (b) under Zn (O) rich conditions in ZnO.

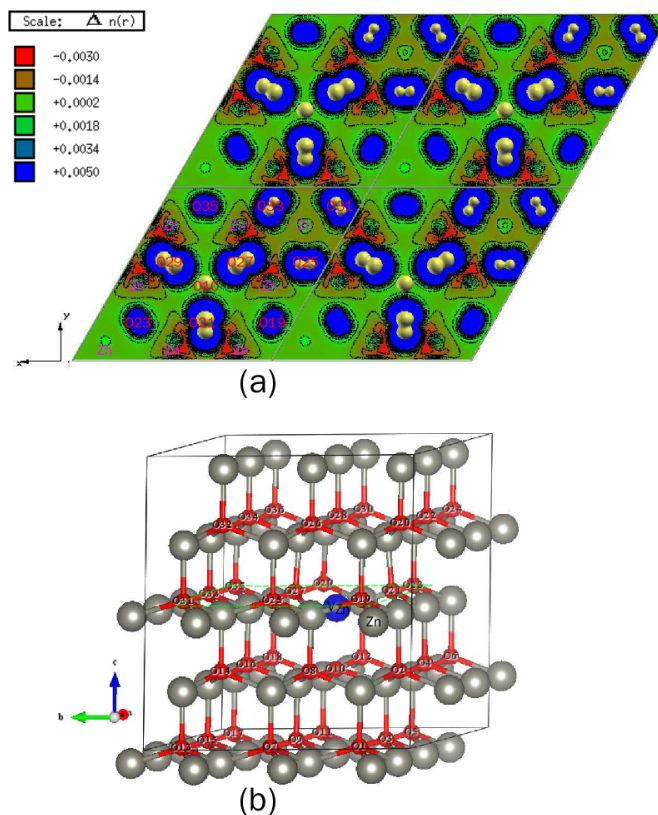


Figure 2: The (000 $\bar{1}$) face spin charge density for ZnO containing a V_{Zn} without biaxial strain is shown in (a), and the isosurface is $0.1e/\text{\AA}^3$. The slice passes through the center of the O atoms surrounding the Zn vacancy, which is labeled by a green dotted line in (b). A constructed $3 \times 3 \times 2$ ZnO supercell is shown in (b), where the blue atom and gray atoms represent the zinc vacancy and Zn atoms, respectively.

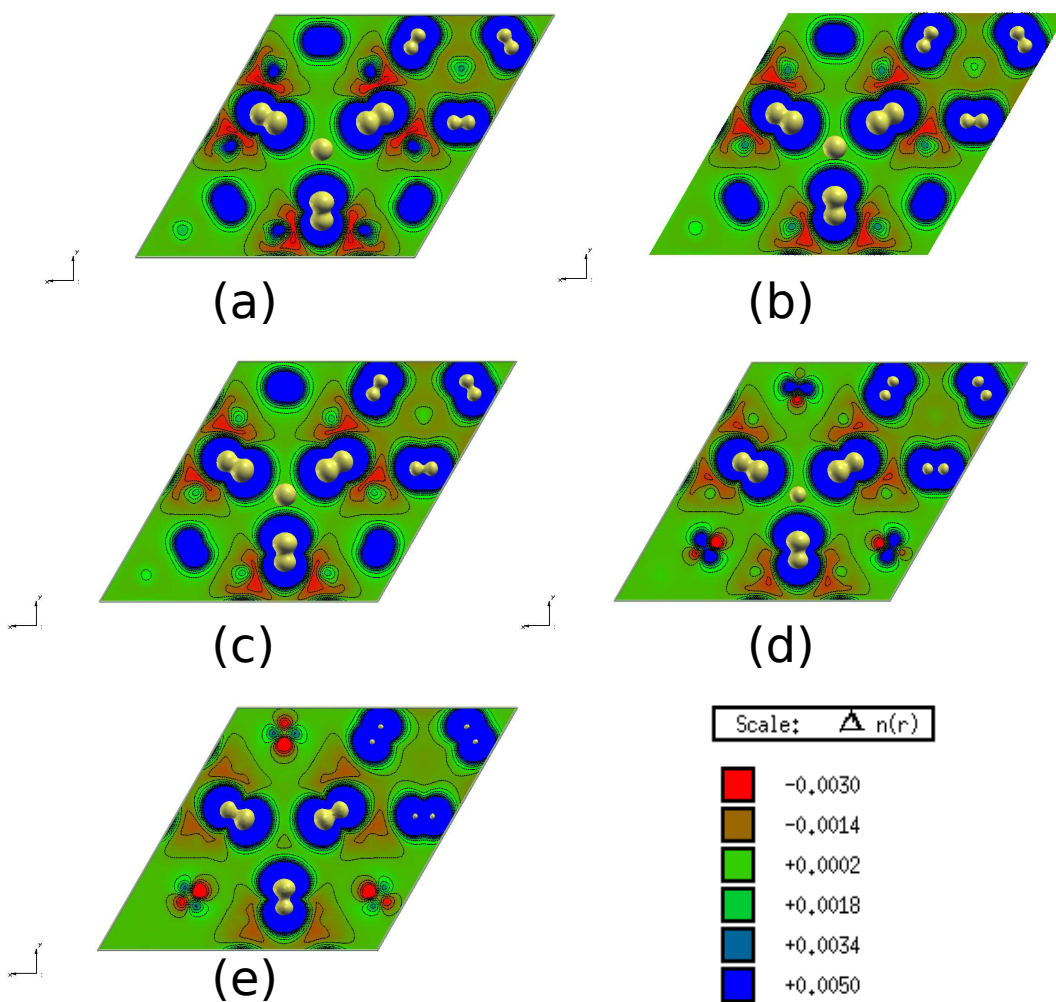


Figure 3: The (0001) face spin charge density for ZnO containing a V_{Zn} with various strain: $\epsilon = -5\%$ (a), $\epsilon = 0\%$ (b), $\epsilon = 1\%$ (c), $\epsilon = 3\%$ (d), and $\epsilon = 5\%$ (e).

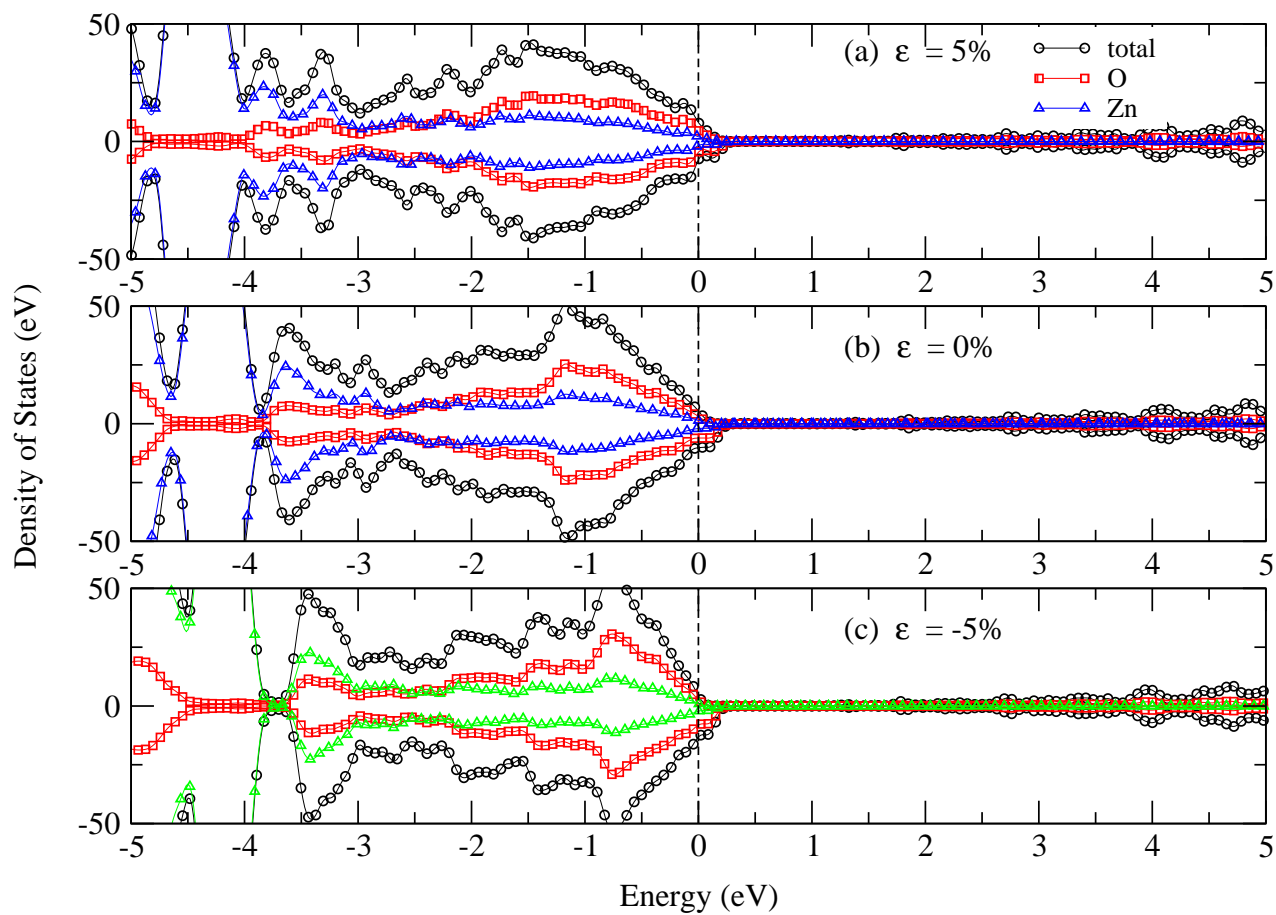


Figure 4: Density of states for ZnO containing a V_{Zn} under various strain: $\epsilon = 5\%$ (a), $\epsilon = 0\%$ (b), and $\epsilon = -5\%$ (c). Positive and negative values are spin-up and spin-down electrons, respectively. The dashed line denotes the Fermi level.

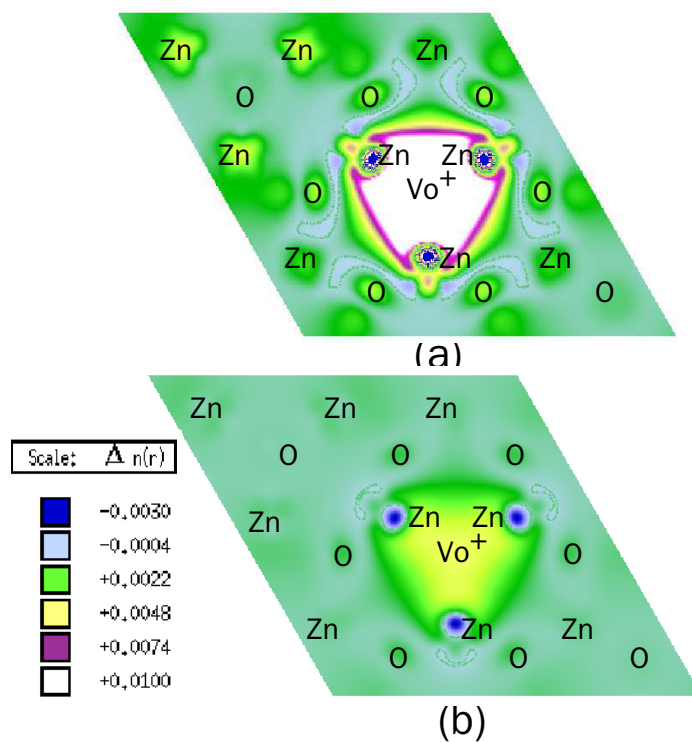


Figure 5: The (0001) face spin charge density for ZnO containing a V_O^+ without strain (a) and with $\epsilon = -1\%$ strain (b). The slices are parallel to the (0001) plane and pass through the centers of the Zn atoms which are the nearest-neighbors of V_O^+ .

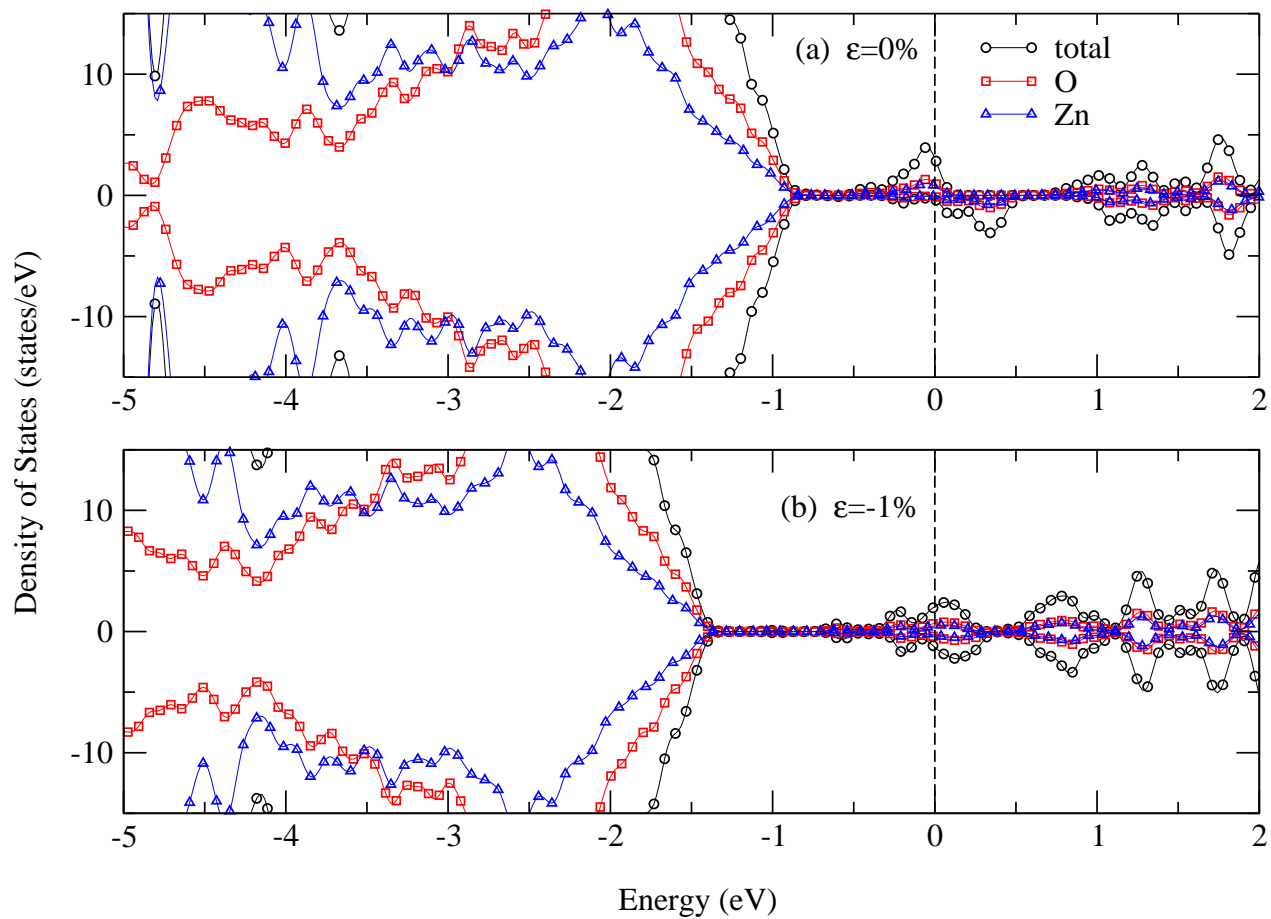


Figure 6: Density of states for ZnO containing a V_O^+ under various strain: $\epsilon = 0\%$ (a) and $\epsilon = -1\%$ (b). Positive and negative values are spin-up and spin-down electrons, respectively. The dashed line denotes the Fermi level.

Table 1: Variation of $E_{FM} - E_{AFM}$ with strain for ZnO with different distance between $2V_{Zn}$ s

strain		-5%	0	3%	5%
$E_{FM} - E_{AFM}$	6.58Å	-109	-72	-41	-29
	9.83Å	-38	-35	-31	-15